of coloboma and visual impairment varied from case to case [Russell-Eggitt et al., 1990].

Recently, the gene *Chromodomain helicase DNA-binding protein-7* (*CHD7*) at chromosome 8q12.1 was identified as a causative gene of CHARGE syndrome [Vissers et al., 2004]. Up to 70% of patients clinically diagnosed as having CHARGE syndrome exhibit mutations in the *CHD7* gene [Aramaki et al., 2006a; Jongmans et al., 2006; Lalani et al., 2006]. Although the exact function of this gene product remains unknown, it may have an important effect on an early stage of ocular morphogenesis.

We conducted the present multicenter study to clarify the ophthalmic features of patients with molecularly confirmed CHARGE syndrome and to explore the role of *CHD7* in ocular development.

PATIENTS AND METHODS

Thirty-eight eyes in 19 patients clinically diagnosed as having CHARGE syndrome at the National Center for Child Health and Development, the Osaka Medical Center and Research Institute for Maternal and Child Health, the Kanagawa Children's Medical Center, or the Institute for Developmental Research, Aichi Human Service Center were retrospectively studied. All the patients had been molecularly confirmed to carry *CHD7* mutations at the Keio University School of Medicine [Aramaki et al., 2006a]. The clinical diagnosis of CHARGE syndrome was made based on the Blake criteria [Blake et al., 1998]. Molecular screening for mutations in the *CHD7* gene was conducted as reported previously [Aramaki et al., 2006b]. Ophthalmic features were examined using slit-lamp biomicroscopy and binocular indirect ophthalmoscopy. Two patients were also examined using a spectral domain optical coherence tomography (SD-OCT). The SD-OCT images were obtained with RS-3000 (NIDEK Co., Ltd., Gamagori, Japan). The best-corrected visual acuity (BCVA) was measured with a standard Japanese VA chart using Landolt rings or pictures at 5 m, then converted to Snellen VA.

The anatomical severity of the eye defect was classified as follows: Grade 1, Normal; Grade 2, colobomata with macular formation; Grade 3, colobomata including the macula; and Grade 4, colobomata, macular defect, and microphthalmos. Then, Cohen's kappa coefficient [Cohen, 1960] was used to measure the agreement of the severity in the two eyes among 19 CHD7-mutation positive patients. The potential correlation between the anatomical severity of the eyes in an individual and the amino acid position where the truncation of the *CHD7* protein occurred in the same individual was evaluated among 14 patients with protein-truncating mutations.

This study was approved by the institutional ethics committee; the patients or the parents of the patients provided informed consent prior to enrollment in the study.

RESULTS

The characteristics of the 38 eyes of the 19 patients with CHARGE syndrome carrying *CHD7* mutations are summarized in Table I. Ten patients (53%) were male and 9 (47%) were female. The age of the patients at the time of the examination ranged from 1 to 21 years (mean 7.9 ± 5.0 years). Ocular abnormalities were found in 18 patients (94.7%), bilateral abnormalities were observed in 17 patients (89.4%), and unilateral abnormalities were observed in 1 patient (5.3%). Among these 18 patients, all 35 abnormal eyes had varying severities of colobomata.

TABLE I. Characteristics of Patients of CHARGE Syndrome With CHD7 Mutations (n = 9)

Variable	Number
Gender	
Male	10 (53%)
Female	9 (47%)
Age at examination	1–21 years
Mean	7.9 ± 5.0 years
Ocular abnormalities (colobomata)	
Bilateral	17 (89.4%)
Unilateral	1 (5.3%)
None	1 (5.3%)
BCVA	
<20/400	4 (21.1%)
20/400 to <20/60	7 (36.8%)
20/60 to 20/20	6 (31.6%)
Not measured	2 (10.5%)

BCVA, best-corrected visual acuity.

The ocular features of the individual patients are summarized in Table II. Colobomata affected the posterior segment in 35/38 eyes (92.1%), retinochoroidal coloboma was present in 33 eyes (86.8%), and optic disk coloboma was present in 33 eyes (86.8%). Both retinochoroidal coloboma and optic disk coloboma were bilaterally present in 15 patients (78.9%) and unilaterally present in 3 patients (15.8%). The coloboma involved the macula totally or partially in 21 eyes (55.3%) of the 13 patients (68.4%): bilaterally in 8 patients

TABLE II. Ocular Features of the Patients (n = 19 patients, 38 eyes)

	Number of patients (%)			
Findings	Bilateral	Unilateral	Total	Number of eyes (%)
Colobomata	17 (89.5)	1 (5.3)	18 (94.7)	35 (92.1)
Retinochoroidal	15 (78.9)	3 (15.8)	18 (94.7)	33 (86.8)
Optic disk	15 (78.9)	3 (15.8)	18 (94.7)	33 (86.8)
Macula	8 (42.1)	5 (26.3)	13 (68.4)	21 (55.3)
Iris	1 (5.3)	0 (0.0)	1 (5.3)	2 (5.3)
Lens	0 (0.0)	1 (5.3)	1 (5.3)	1 (2.6)
Microphthalmos	3 (15.8)	2 (10.5)	5 (26.3)	8 (21.1)
Microcornea	3 (15.8)	1 (5.3)	4 (21.1)	7 (18.4)
Ptosis	1 (5.3)	1 (5.3)	2 (10.5)	3 (7.9)
PFV	0 (0.0)	1 (5.3)	1 (5.3)	1 (2.6)
Cataract	0 (0.0)	1 (5.3)	1 (5.3)	1 (2.6)
High myopia (>6.0 D)	2 (10.5)	1 (5.3)	3 (15.8)	5 (13.2)

PFV, persistent fetal vasculature.

(42.1%) and unilaterally in 5 patients (26.3%). The SD-OCT demonstrated a partially formed macula and cystic changes in the colobomatous area in 1 case (Fig. 1).

Only 2 eyes of 1 patient (5.3%) were identified as having iris colobomata, and 1 eye (2.6%) of another patient was revealed by examination under general anesthesia to have a dislocated and colobomatous lens. No cases of eyelid colobomata were seen, but congenital ptosis was present in 3 eyes (7.9%) of 2 patients who had undergone surgical treatment. All the cases of ptosis were not pseudoptosis associated with microphthalmos and/or cranial nerve palsy, but were true congenital ptosis associated with poor levator function. We evaluated the levator muscle function in each case. None of the patients had a history of acquired causes or signs of oculomotor palsy, such as paralytic strabismus and limited ocular movement.

Microphthalmos was found in 8 eyes (21.1%) of 5 patients (26.3%): bilaterally in 3 patients (15.8%) and unilaterally in 2 patients (10.5%). Microcornea was also present in 7 eyes (18.4%) of 4 patients (21.1%): bilaterally in 3 patients (15.8%) and unilaterally in 1 patient (5.3%). Persistent fetal vasculature was identified in 1 eye (2.6%). Cataracts had developed in 1 eye (2.6%), but neither glaucoma nor retinal detachment was observed in this series.

The refraction could be estimated in 23 eyes of 12 patients (63.2%). Of these eyes, 10 were myopic, 7 were emmetropic, and 6 were hypermetropic. High myopia (−6.00 diopters or more) was found in 5 eyes (13.2%) of 3 patients (15.8%).

The BCVA are shown in Table I. The measurement of VA was possible in 17 patients (89.5%) older than 3 years of age. The remaining 2 patients were infants or mentally retarded. The binocular BCVA or BCVA in the better eye was less than 20/400 in 4 patients (21.1%), less than 20/60 but no less than 20/400 in 7 patients (36.8%), and 20/60 to 20/20 in 6 patients (31.6%) with macular formation (Fig. 1). The overall prevalence of blindness and visual impairment (less than 20/60) [World Health Organization, 1992] among the 17 patients was 65%.

The agreement of anatomical severity between the 2 eyes in each of the 19 patients was evaluated using Cohen's Kappa statistics. The κ statistic of 0.41 suggested a moderate degree of agreement, per the guidelines by Landis and Koch [1977]. Because there was a moderate, if not a substantial, agreement between the severity of the 2 eyes, the severity grading of the more severely affected eye was used as the representative grade for the severity of the eyes in an individual. The correlation between the anatomical severity of the eyes in an individual and the amino acid position where the truncation of the CHD7 protein occurred in the same individual is illustrated in Figure 2. Patients with truncated protein devoid of the SANT domain tended to have severer anatomical defects of the eyes. Subcategorization of the patients according to the presence or absence of the SANT domain (4 cases with intact SANT domain and 10 other cases), and the subcategorization of the anatomical severity of the eyes in an individual (7 cases classified as Grade 1 or 2 vs. 7 cases classified as Grade 3 or 4) revealed a statistically

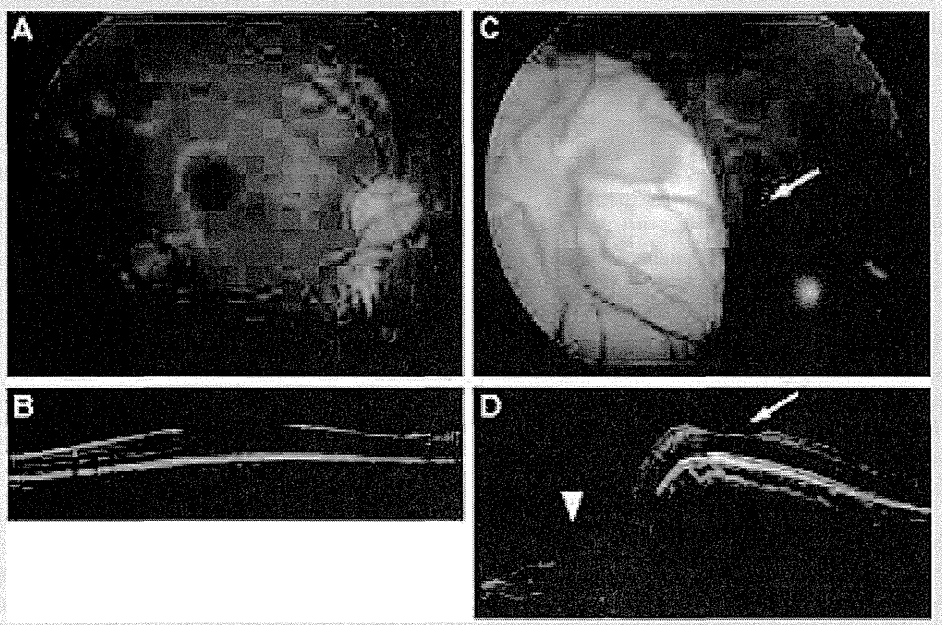

FIG. 1. Fundus photographs and spectral domain optical coherence tomography (SD-OCT) scan of the retina in the right eye (A,B) and the left eye (C,D) in a 6-year-old girl. A: Retinochoroidal colobomata inferior to the optic disk is visible in the right eye. B: The SD-OCT shows a good macular formation in the right eye, resulting in a BCVA of 20/20. C: Retinochoroidal and optic disk coloboma are seen in the left eye. The colobomata partially involved the macula (arrow). D: The SD-OCT shows a partially formed macula (arrow) and cystic changes in the colobomatous area (arrow head) in the left eye, resulting in a BCVA of 20/50 after amblyopia treatment.

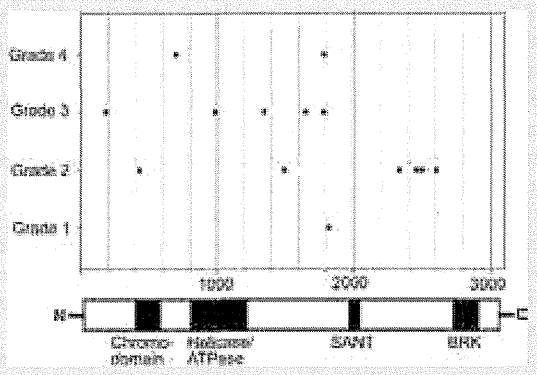

FIG. 2. The correlation between the anatomical severity of the eyes in an individual and the amino acid position where the truncation of the CHD7 protein occurred in the same individual. Horizontal axis indicates amino acid position of the CHD7 protein together with the domains of the protein. Vertical axis indicates the anatomical severity of the eye defect classified as follows: Grade 1, Normal; Grade 2, colobomata with macular formation; Grade 3, colobomata including the macula; and Grade 4, colobomata, macular defect, and microphthalmos.

significant correlation between the location of protein truncation and the anatomical severity of the eyes ($P = 0.02$, chi-squared test).

DISCUSSION

In the current series, the incidence of coloboma, the major ocular feature of CHARGE syndrome, was 94.7% (18/19), which was much higher than the previously reported incidence. Since most of the authors were ophthalmologists, the number of cases without eye defects might have been underrepresented. Hence, this high incidence should be viewed with caution. Nevertheless, attending clinical geneticists were on duty at all the participating children's hospitals, and thus the bias from such underrepresentation may be relatively small. The finding that there was one mutation-positive patient who did not have abnormal eye findings confirms that no finding in CHARGE syndrome has a 100% penetrance as is sometimes surmised.

Both retinochoroidal and optic disk coloboma occurred in 94.7% of the cases, mostly bilaterally, while the incidence of iris coloboma was only 5.3% (1/19). Coloboma also affected the macula in 68.4% of the cases. We confirmed that bilateral large retinochoroidal colobomata represent a typical ophthalmic feature of CHARGE syndrome with *CHD7* mutations.

The incidence of anomalies in the anterior segment was lower than that in the posterior segment, although microphthalmos, microcornea, PFV, and cataracts were present in some cases bilaterally or unilaterally. The presence of characteristic large retinochoroidal coloboma indicates the essential role of *CHD7* in the closure of the fetal fissure posteriorly between 5 and 6 weeks of gestation, and the malfunction of *CHD7* may have an effect so severe as to influence the entire ocular morphogenesis to some degree. Although most cases had bilateral colobomata in the posterior segment, the severity and associated features often differed between the two eyes. Other associated features in this series were ptosis in 10.5% and high myopia in 15.8%. Subtle-associated anomalies and refractive errors may have been underestimated in examinations that were not performed under general anesthesia.

The anatomical severity grading of the eye defect was evaluated in two ways: a comparison between the severity in one eye in comparison with that in the other eye and the correlation between the severity and the genotype. The low-to-moderate degree of agreement between the two eyes (i.e., left and right) reflects the general facial asymmetry in patients with CHARGE syndrome [Zentner et al., 2010]. In other words, the lack of substantial or perfect agreement between the anatomical severity of the right and the left eyes indicates a variable phenotypic effect of the same mutation. Yet, the location of protein truncation and the anatomical severity of the eyes were significantly correlated: if the chromodomain, helicase/ATP domain, and SANT domains are intact, the severity of the eyes tends to be milder. Interestingly, all four cases in which those domains were intact had less severe eye defects with intact macula. Further studies are warranted to verify this potential genotype–phenotype correlation.

The visual acuities of the eyes ranged between no light perception and 20/20, and the prevalence of blindness and visual impairment (less than 20/60) was 65% among 17 patients. A poor visual prognosis depended on the presence of a large coloboma involving the macula in the posterior segment and associated microphthalmos or microcornea, as reported previously [Russell-Eggitt et al., 1990; Hornby et al., 2000]. On the other hand, even eyes with large colobomata as a result of *CHD7* mutations were capable of forming maculas, resulting in good central visual acuity with superior visual field defects. As shown in the case illustrated in Figure 1, even a partially formed macula will enable useful vision following the adequate treatment of amblyopia as optical correction and patching during the earlier age of visual development. A recent report of a case examined using OCT revealed additional morphologic characteristics of eyes in patients with CHARGE syndrome carrying *CHD7* mutations [Holak et al., 2008]. Further investigation of retinal morphology and function using OCT and electroretinograms (ERG) may help to clarify the function of *CHD7* in ocular morphogenesis, including macular formation.

We suggested that the early diagnosis of retinal morphology and function, especially of macular lesions by way of OCT and ERG, may be beneficial to patients, since such attention may determine whether treatment for amblyopia, such as optical correction and patching, will be effective in facilitating the visual potential or whether care for poor vision will be needed. An infant's visual acuity rapidly develops during its first 2–3 years and continues up until 7–8 years of age, but plasticity decreases progressively thereafter. Thus, a better visual prognosis can be obtained with the earlier treatment of amblyopia during the critical period of visual development.

ACKNOWLEDGMENTS

This study was supported by the Health and Labour Sciences Research Grants of Research on Intractable Diseases from the Ministry of Health, Labour and Welfare, Tokyo, Japan.

REFERENCES

Aramaki M, Udaka T, Kosaki R, Makita Y, Okamoto N, Yoshihashi H, Oki H, Nanao K, Moriyama N, Oku S, Hasegawa T, Takahashi T, Fukushima Y, Kawame H, Kosaki K. 2006a. Phenotypic spectrum of CHARGE syndrome with CDH7 mutations. J Pediatr 148:410–414.

Aramaki M, Udaka T, Torii C, Samejima H, Kosaki R, Takahashi T, Kosaki K. 2006b. Screening for CHARGE syndrome mutations in the CDH7 gene using denaturing high-performance liquid chromatography. Genet Test 10:244–251.

Blake KD, Davenport SL, Hall BD, Hefner MA, Pagon RA, Williams MS, Lin AE, Graham JM Jr. 1998. CHARGE association: An update and review for the primary pediatrician. Clin Pediatr (Phila) 37:159–173.

Cohen J. 1960. A coefficient of agreement for nominal scales. Educ Psychol Meat 20:37–46.

Holak HM, Kohlhase J, Holak SA, Holak NH. 2008. New recognized ophthalmic morphologic anomalies in CHARGE syndrome caused by the R2319C mutation in the CHD7 gene. Ophthalmic Genet 29:79–84.

Hornby SJ, Adolph S, Girbert CE, Dandona L, Foster A. 2000. Visual acuity in children with coloboma. Clinical features and a new phenotypic classification system. Ophthalmology 107:511–520.

Jongmans MC, Admiraal RJ, van der Donk KP, Vissers LE, Baas AF, Kapusta L, van Hagen JM, Donnai D, de Ravel TJ, Veltman JA, van Kessel AG, De Vries BB, Brunnaer HG, Hoefsloot LH, van Ravenswaaj CM. 2006. CHARGE syndrome: The phenotypic spectrum of mutations in the CHD7 gene. J Med Genet 43:306–314.

Lalani SR, Saliullah AM, Fernbach SD, Harutyunyan KG, Thaller C, Peterson LE, McPherson JD, Gibbs RA, White LD, Hefner M, Davenport SLH, Graham JM Jr, Bacino CA, Glass NL, Towbin JA, Craigen WJ, Neish SR, Lin AE, Belmont JW. 2006. Spectrum of CHD7 mutations in 110 individuals with CHARGE syndrome and genotype–phenotype correlation. Am J Hum Genet 78:303–314.

Landis JR, Koch GG. 1977. The measurement of observer agreement for categorical data. Biometrics 33:159–174.

Pagon RA, Graham JM Jr, Zonana J, Yong SL. 1981. Coloboma, congenital heart disease, and choanal atresia with multiple anomalies: CHARGE association. J Pediatr 99:223–227.

Russell-Eggitt IM, Blake KD, Taylor DSI, Wyse RKH. 1990. The eye in the CHARGE association. Br J Ophthalmol 74:421–426.

Vissers LE, van Ravenswaaij CM, Admiraal R, Hurst JA, de Vries BB, Janssen IM, van der Vliet WA, Huys EH, de Jong PJ, Hamel BC, Schoenmakers EF, Brunner HG, Veltman JA, van Kessel AG. 2004. Mutations in a new member of the chromodomain gene family cause CHARGE syndrome. Nat Genet 36:955–957.

World Health Oraganization. 1992. International statistical classification of diseases and related problems. 10th revision. Vol. 1. Geneva, Switzerland: World Health Organization.

Zentner GE, Layman WS, Martin DM, Scacheri PC. 2010. Molecular and phenotypic aspects of CHD7 mutation in CHARGE syndrome. Am J Med Genet Part A 152A:674–686.

CLINICAL GENETICS An International Journal of Genetics, Molecular and Personalized Medicine

Clin Genet 2013: 83: 135–144
Printed in Singapore. All rights reserved

Published by Blackwell Publishing Ltd
CLINICAL GENETICS
doi: 10.1111/j.1399-0004.2012.01885.x

Original Article

Exome sequencing in a family with an X-linked lethal malformation syndrome: clinical consequences of hemizygous truncating *OFD1* mutations in male patients

Tsurusaki Y, Kosho T, Hatasaki K, Narumi Y, Wakui K, Fukushima Y, Doi H, Saitsu H, Miyake N, Matsumoto N. Exome sequencing in a family with an X-linked lethal malformation syndrome: clinical consequences of hemizygous truncating *OFD1* mutations in male patients.
Clin Genet 2013: 83: 135–144. © John Wiley & Sons A/S. Published by Blackwell Publishing Ltd, 2012

Oral-facial-digital syndrome type 1 (OFD1; OMIM #311200) is an X-linked dominant disorder, caused by heterozygous mutations in the *OFD1* gene and characterized by facial anomalies, abnormalities in oral tissues, digits, brain, and kidney; and male lethality in the first or second trimester pregnancy. We encountered a family with three affected male neonates having an 'unclassified' X-linked lethal congenital malformation syndrome. Exome sequencing of entire transcripts of the whole X chromosome has identified a novel splicing mutation (c.2388+1G > C) in intron 17 of *OFD1*, resulting in a premature stop codon at amino acid position 796. The affected males manifested severe multisystem complications in addition to the cardinal features of OFD1 and the carrier female showed only subtle features of OFD1. The present patients and the previously reported male patients from four families (clinical OFD1; Simpson-Golabi-Behmel syndrome, type 2 with an *OFD1* mutation; Joubert syndrome-10 with *OFD1* mutations) would belong to a single syndrome spectrum caused by truncating OFD1 mutations, presenting with craniofacial features (macrocephaly, depressed or broad nasal bridge, and lip abnormalities), postaxial polydactyly, respiratory insufficiency with recurrent respiratory tract infections in survivors, severe mental or developmental retardation, and brain malformations (hypoplasia or agenesis of corpus callosum and/or cerebellar vermis and posterior fossa abnormalities).

Conflict of interest

The authors have no conflict of interest to declare.

Y Tsurusaki[a]*, T Kosho[b]*, K Hatasaki[c], Y Narumi[b], K Wakui[b], Y Fukushima[b], H Doi[a], H Saitsu[a], N Miyake[a] and N Matsumoto[a]

[a]Department of Human Genetics, Yokohama City Graduate School of Medicine, Yokohama, Japan, [b]Department of Medical Genetics, Shinshu University School of Medicine, Matsumoto, Japan, and [c]Department of Pediatrics, Toyama Prefectural Central Hospital, Toyama, Japan

*These authors contributed equally to this work.

Key words: exome sequencing – OFD1 – *OFD1* gene – splicing mutation – X-linked congenital malformation syndrome

Corresponding authors: Tomoki Kosho, MD, Department of Medical Genetics, Shinshu University School of Medicine, 3-1-1 Asahi, Matsumoto, Nagano 390-8621, Japan.
Tel.: +81 263 37 2618;
fax: +81 263 37 2619;
e-mail: ktomoki@shinshu-u.ac.jp
and
Naomichi Matsumoto, MD, PhD, Department of Human Genetics, Yokohama City Graduate School of Medicine, 3-9 Fukuura, Kanazawa-ku, Yokohama 236-0004, Japan.
Tel.: +81 45 787 260;
fax: +81 45 786 5219;
e-mail: naomat@yokohama-cu.ac.jp

Received 14 January 2012, revised and accepted for publication 26 March 2012

Oral-facial-digital syndrome type 1 (OFD1; OMIM #311200), originally described by Papillon-Leage and Psaume (1) and further delineated by Gorlin and Psaume (2), is an X-linked dominant developmental disorder with an estimated prevalence of 1:50,000, caused by mutations in the *OFD1* gene (OMIM #300170) (3–5). The disorder is characterized by facial anomalies and abnormalities in oral tissues, digits, brain and kidney (5). Almost all affected individuals with OFD1 are female, with highly variable expression, possibly resulting from random X inactivation (6). Affected males are generally lost in the first or second trimester of pregnancy (4). To date, only one liveborn male case with clinically definite OFD1 and a normal karyotype has been reported; the patient was born at 34 weeks of gestation and died 21 h after birth due to heart failure (7). In this report, we describe a family with three affected male neonates having an 'unclassified' X-linked lethal congenital malformation syndrome. Exome sequencing of entire transcripts of the whole X chromosome has successfully identified a causative splicing mutation in *OFD1*.

Subjects and methods

Clinical report

II-2, a 22-year-old woman, was referred to our clinic for genetic counseling (Fig. 1). Her deceased brother (II-4) had severe multiple congenital abnormalities. She had two sons (III-1 and III-5) with similar congenital abnormalities and a healthy boy (III-3) as well as two miscarriages (III-2, artificial; III-4, spontaneous). During genetic counseling and molecular investigations, she had another healthy boy (III-5). After identification of a heterozygous *OFD1* mutation, she was examined for features of OFD1. Only a few accessory frenulae and irregular teeth with no facial anomalies or tongue abnormalities were observed (Fig. 2a–e). A radiograph of her hands showed no abnormalities (Fig. 2f) and an abdominal ultrasonography detected no cysts in the kidneys, liver, or pancreas (data not shown). I-2, allegedly, had no apparent malformations or complications including renal diseases.

II-4 was born by caesarean section because of placental abruption at 33 weeks of gestation. Pregnancy was complicated by polyhydramnios. Apgar score was 3 at 1 min. His birth weight was 2056 g (+0 SD), length was 45.0 cm (+0.5 SD), and occipitofrontal circumference (OFC) was 34.0 cm (+2.0 SD). He manifested severe respiratory insufficiency and was transferred to a neonatal intensive care unit (NICU). His craniofacial features included a prominent forehead, a large fontanelle (5 × 5 cm), a low posterior hairline, microphthalmia, hypertelorism, short palpebral fissures, depressed nasal bridge, low-set ears, a small cleft lip and a soft cleft palate, narrowing of the tip of the tongue, and a hypoplastic gum (Fig. 2g). Additional physical features included redundant neck skin, postaxial polydactyly of the left hand (Fig. 2h), wide halluces (Fig. 2i), micropenis, and left cryptorchidism.

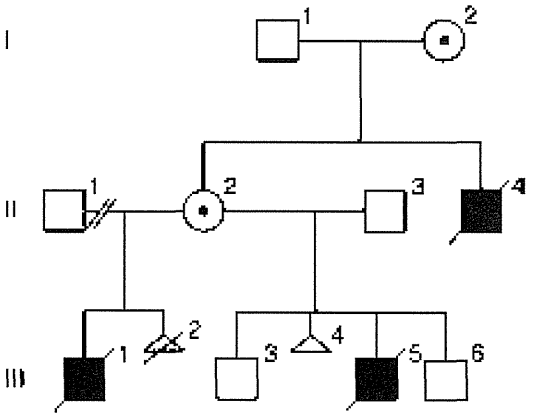

Fig. 1. Familial pedigree.

Ultrasonography revealed hypoplastic gyri, an atrial septal defect, and patent ductus arteriosus. Ophthalmological examination detected microcornea and retinal detachment. Intubation was impossible because of laryngeal anomalies and the patient died 11 h after birth. Additional autopsy findings included partial atelectasis and bilateral hydroureters.

III-1 was delivered by emergency caesarean section at 39 weeks of gestation. Pregnancy was complicated by polyhydramnios and intrauterine growth retardation, with moderate macrocephaly. His birth weight was 3064 g (+0.1 SD). He was admitted to a NICU because of respiratory insufficiency, and received mechanical ventilation. His craniofacial features included microphthalmia, hypertelorism, short palpebral fissures, epicanthus, low-set ears, and a cleft lip and palate. Additional physical features included bilateral polydactyly of hands (postaxial) and feet (preaxial), and an ectopic urethral opening. Ultrasonography revealed hydrocephalus, agenesis of the corpus callosum and cerebellar vermis, and a complete atrioventricular septal defect. Ophthalmological examination detected persistent pupillary membrane and optic disc coloboma. G-banded chromosomes were normal (46,XY). The patient died at age 14 days due to heart failure.

III-5 was delivered by caesarean section at 32 weeks of gestation. Pregnancy was complicated by polyhydramnios, intrauterine growth retardation, and congenital heart defects. His birth weight was 1704 g (−0.2 SD), length was 40.0 cm (−0.8 SD), and OFC was 33.3 cm (+2.0 SD). He was admitted to a NICU because of respiratory insufficiency, and received mechanical ventilation. His craniofacial features included a prominent forehead, hypertelorism, dysplastic ears, a small cleft lip, and a soft cleft palate (Fig. 2j,k). Ultrasonography revealed hydrocephalus with Dandy-Walker malformation and hypoplastic left heart syndrome. G-banded chromosomes were normal (46,XY). The patient died 1 day after birth. Additional autopsy findings included agenesis of the cerebellar vermis (Fig. 2l), enlargement of the fourth ventricle and aqueduct, anomalous positioning of the esophagus, mild

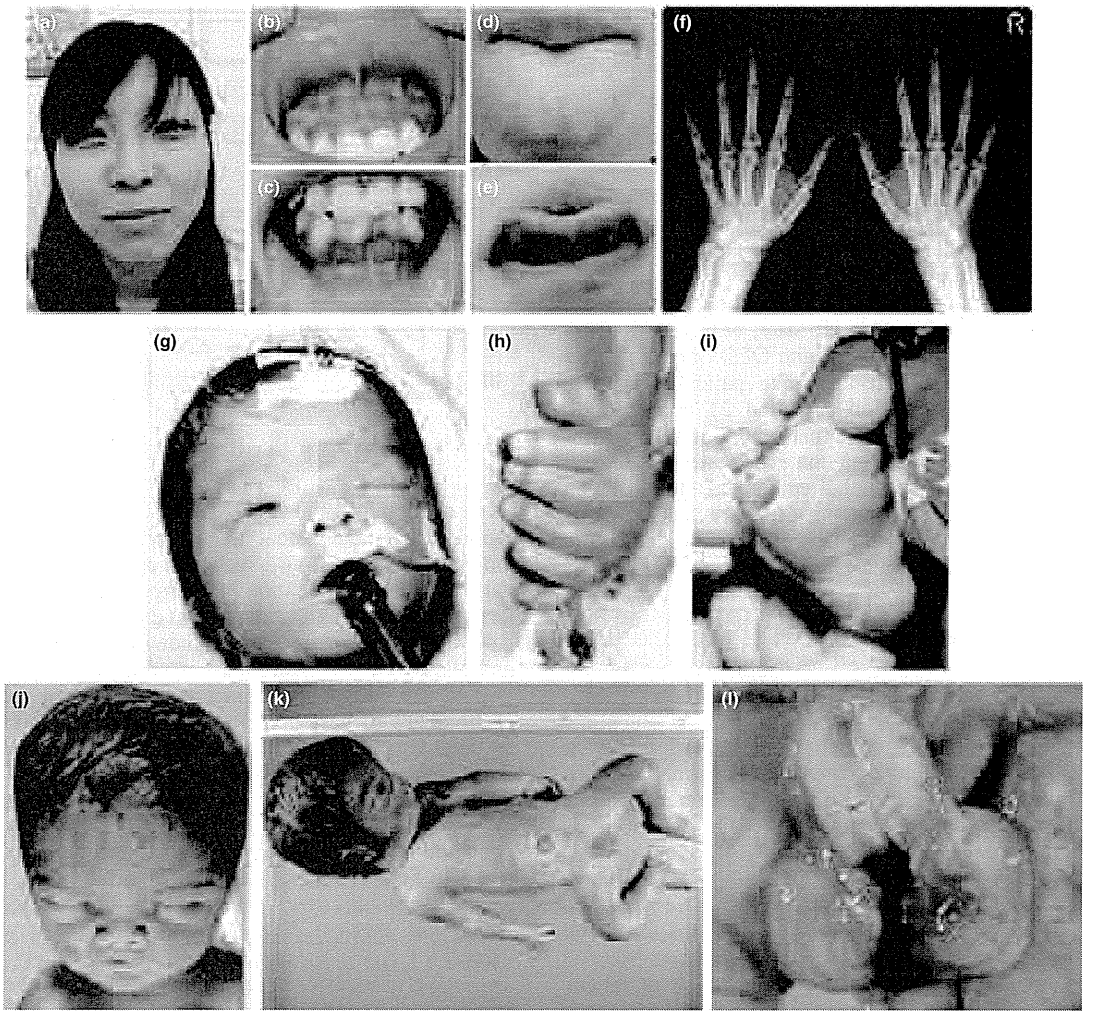

Fig. 2. Clinical photographs of II-2 (**a–f**), II-4 (**g–i**), and III-5 (**j–l**).

pulmonary congestion, and insufficient lobulation of the right lung.

The three affected male neonates, having strikingly similar clinical manifestations (Table 1), are considered to have had a congenital malformation syndrome with X-linked inheritance. Array-CGH analysis using 4200 BAC clones identified no pathologic genomic copy number abnormalities. Direct sequencing of *MID*, performed because of a partial similarity to these neonates' syndrome to X-linked Opitz-G/BBB syndrome (OMIM #300000) (8), revealed no mutation.

Library preparation

Genomic DNA for II-2, II-3, III-3, and III-6 was extracted from peripheral blood using the Gentra PureGene Blood Kit (QIAGEN, Hilden, Germany), and genomic DNA for III-5 was extracted from the preserved dried umbilical cord using the DNeasy Blood & Tissue Kit (QIAGEN). Three micrograms of high-quality (absorbance at 260 nm/absorbance at 280 nm: 1.8–2.0) genomic DNA from II-2 was fragmented using the Covaris model S2 system (Covaris, Woburn, MA). The target peak size was 150 bp. After the size of sheared DNA was checked using an Agilent 2100 Bioanalyzer (Agilent Technologies, Santa Clara, CA), adapter sequences were ligated to the ends of DNA fragments, and amplified according to the manufacturer's protocol (Agilent Technologies).

Exome capture and next-generation sequencing

Library DNA was hybridized for 24 h at 65°C using the SureSelect Human X Chromosome Demo Kit (Agilent Technologies). Captured DNA was diluted to a concentration of 8 pM and sequenced on a Genome Analyzer IIx (Illumina, San Diego, CA) with 76-bp paired-end reads. We used only one of the eight lanes in the flow

Table 1. Variant priority scheme after exome sequencing[a]

	NEXTGENE	II-2	MAQ (SEATTLESEQ)
Total variants called	22,176	—	58,081
Chr X	3441	—	4383
Unknown SNP variants	910	—	882
(dbSNP131, 1000 genomes)	—	—	—
Overlap of NEXTGENE and MAQ	—	169	—
NS/SS	—	17	—
Except for variants at segmental duplications	—	15	—

NS, non-synonymous; SNP, single-nucleotide polymorphism; SS, splice site (±2).
[a]MAQ was annotated with SEATTLESEQ ANNOTATION. The annotation includes gene names, dbSNP rs ID, and SNP functions (e.g. missense), protein positions and amino acid changes.

cell for II-2 (Illumina). Image analyses and base calling were performed using sequence control software real-time analysis and OFFLINE BASECALLER software v1.8.0 (Illumina). Reads were aligned to the human reference genome (UCSC hg19, NCBI build 37.1).

Mapping strategy and variant annotation

The quality-controlled (Path Filter) reads were mapped to the human reference genome (UCSC hg19, NCBI build 37.1), using mapping and assembly with quality (MAQ) and NEXTGENE software v2.0 (SoftGenetics, State College, PA). Single-nucleotide polymorphisms in MAQ-passed reads were annotated using the SEATTLESEQ ANNOTATION website (http://gvs.gs.washington.edu/SeattleSeqAnnotation/).

Priority scheme and capillary sequencing

Called variants found by each informatics method were filtered in terms of location on chromosome X, unregistered variants (excluding registered dbSNP131 and 1000 Genomes), overlapping variants called in common by NEXTGENE and MAQ, and non-synonymous changes and splice-site mutations (±2 bp from exon–intron junctions) (Table 1). The variants were confirmed as true positives by Sanger sequencing of polymerase chain reaction (PCR) products amplified using genomic DNA as a template, except for variants within genes at segmental duplications. Sanger sequencing was performed on an ABI3500xl or ABI3100 autosequencer (Life Technologies, Carlsbad, CA). Sequencing data were analyzed using SEQUENCHER software (Gene Codes Corporation, Ann Arbor, MI).

Reverse transcription-PCR

Total RNA was isolated from EBV-transformed lymphoblastoid cell line (EBV-LCL) derived from II-2 and healthy control subjects using the RNeasy Plus Mini Kit (QIAGEN). Five micrograms of total cellular RNA was used for reverse transcription with the Super Script III First-Strand Synthesis System (Life Technologies). Two microliters of synthesized complementary DNA was used for PCR with the following primers: ex17-F (5′-CTACCATCACCCACTGAGTC-3′) and ex19-R (5′-TGAGACATATCCCCGGCAG-3′). Amplified PCR products were electrophoresed in agarose gels, purified from gels using the QIAquick Gel Extraction Kit (QIAGEN), cloned into pCR4-TOPO vector (Life Technologies) and sequenced.

X-chromosome inactivation assay

The human androgen receptor (HUMARA) assay was performed as previously reported (9). Genomic DNA of II-2 was digested at 37°C for 18 h with two methylation-sensitive enzymes, *Hpa*II and *Hha*I. PCR was performed using digested and undigested DNA with HUMARA primers (FAM-labeled ARf: 5′-TCCAGAATCTGTTCCAGAGCGTGC-3′; ARr: 5′-CTCTACGATGGGCTTGGGGAGAAC-3′). DNA fragment analysis was performed on an ABI3130xl autosequencer (Life Technologies). Fragment data were analyzed with GENEMAPPERT SOFTWARE version 4.1 (Life Technologies).

Results

Exome sequencing

Because this disorder was assumed to be an 'X-linked recessive' disorder based on the initial pedigree information, we focused on the X chromosome. Approximately 4.5 Gb of sequence data were generated, 87.3% of which was mapped to the human reference genome (UCSC hg19, NCBI build 37.1). MAQ was able to align 53,242,972 reads to the whole genome.

Two informatics methods identified 17 potential pathogenic changes (15 missense mutations, 1 nonsense mutation, and 1 splice-site mutation) (Table 1). The nonsense mutation was a false positive and all 13 missense mutations were inconsistent with the phenotype (no co-segregation). The mutation c.2388+1G>C was identified at the splice-acceptor site of intron 17 in *OFD1*, heterozygously in II-2, and hemizygously in III-5, but was absent in II-3, III-3, and III-6 (Fig. 3a) as well as 93 normal female controls (0/186 alleles).

RT-PCR, direct sequencing

To examine the mutational effects of c.2388+1G>C, reverse transcriptase-polymerase chain reaction (RT-PCR) was performed. Only a 239-bp PCR product (wild-type allele) was observed in healthy control individuals (Fig. 3b). By contrast, a longer 1364-bp product was detected in II-2. Sequencing of the 1364-bp product revealed that a 1125-bp sequence of intron 17 was retained, producing a premature stop codon at amino acid position 796 (Fig. 3b). These data indicate

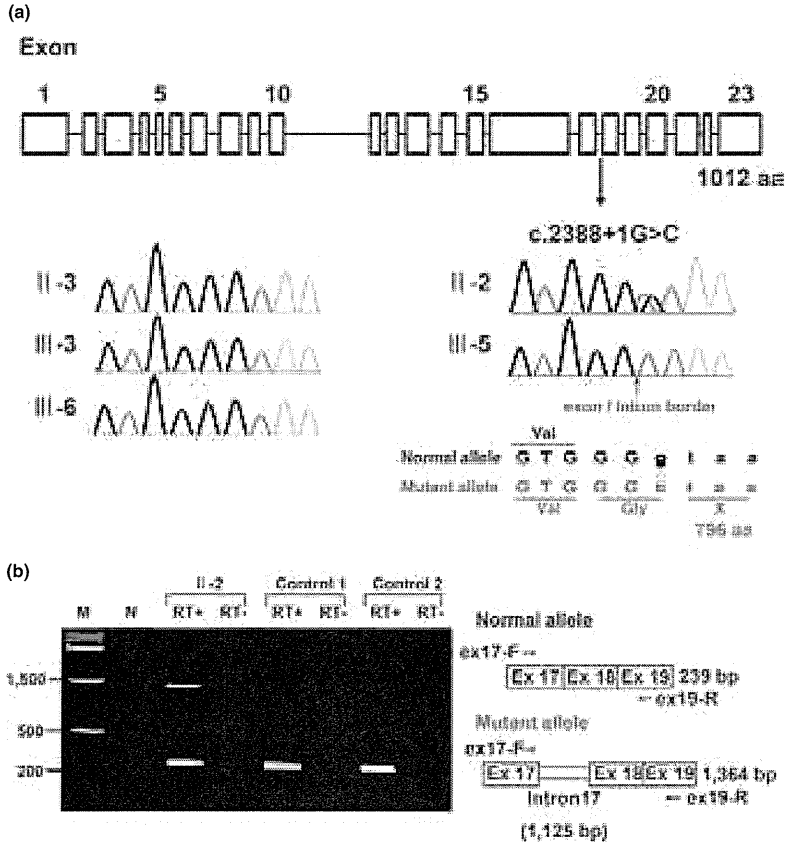

Fig. 3. (**a**) Gene structure of *OFD1* with the mutation (c.2388+1G>C) (upper). Electropherograms of the family members. Wild-type sequences are seen in II-3, III-3 and III-6. Heterozygous and hemizygous mutations are observed in II-2 and III-5, respectively. (**b**) Reverse transcriptase-polymerase chain reaction analysis showing both 239-bp and 1364-bp products in II-2, and only 239-bp products in two normal female controls. The 239-bp product is normal and the 1364-bp product is aberrant.

that the c.2388+1G>C mutation in *OFD1* is most likely the causal mutation in this family.

X-chromosome inactivation assay

X-chromosome inactivation patterns was random patterns in II-2 available for this study (ratio > 38:62).

Discussion

Exome sequencing detected a single-base substitution (c.2388+1G>C) in *OFD1*, resulting in an error in splicing of intron 17 and a premature stop codon at amino acid position 796, in an affected male (III-5) and a carrier female (II-2) in this family with an 'unclassified' X-linked lethal congenital malformation syndrome. II-4 and III-1, who had strikingly similar clinical manifestations to III-5, are likely to have had the same *OFD1* mutation as III-5, although their DNA was not available. Through reassessment of clinical features of the family, the three affected males shared facial, oral, and digital malformations characteristic of OFD1 (4). Additionally, they exhibited more severe complications in various systems including congenital heart defects, genitourinary malformations, and ophthalmological abnormalities. II-2 was also found to have subtle features of OFD1 (accessory frenulae and irregular teeth). Thus, we have concluded that the 'unclassified' X-linked lethal congenital malformation syndrome in this family was clinically compatible with OFD1.

An *OFD1* mutation (c.2123_2126dupAAGA in exon 16, p.Asn711Lysfs*3) was also detected in a family with an X-linked recessive mental retardation syndrome (10). Nine affected males had macrocephaly and severe mental or developmental retardation, and suffered from recurrent respiratory tract infections leading to early death in eight. Only an 11-year-old boy survived with severe mental retardation (IQ 20), obesity, and brachydactyly. His younger brother had postaxial polydactyly. No cognitive, oral, facial, digital, or renal abnormalities were detected in heterozygous carrier females in that family. The patients were later classified into an infantile lethal variant of Simpson-Golabi-Behmel syndrome (type 2) (SGBS2, OMIM #300209), which had consisted of only one family,

genetically mapped to Xp22, including four maternally related affected males with hydrops at birth, craniofacial anomalies (macrocephaly, low-set posteriorly angulated ears, hypertelorism, short and broad nose with anteverted nares, large mouth with thin upper vermilion border, prominent philtrum, high-arched or cleft palate, and short neck), redundant skin, hypoplastic nails, skeletal defects involving upper and lower limbs, gastrointestinal and genitourinary anomalies, hypotonia and neurological impairment, and early death within the first 8 weeks (11, 12). Other *OFD1* mutations were detected in two families with Joubert syndrome-10 (JBTS10, OMIM #213300) (13). A mutation (c.2844_2850delAGACAAA in exon 21, p.Lys948Asnfs*9) in a family with eight affected males caused severe mental or developmental retardation and recurrent infections in all; postaxial polydactyly in five, retinitis pigmentosa in three, and a molar tooth sign on brain magnetic resonance imaging (MRI) in two. No heterozygous carrier females had any symptoms similar to those in the affected males. Another mutation (c.2767delG in exon 21, p.Glu923Lysfs*4) was found *de novo* in a 12-year-old male patient with severe mental retardation, macrocephaly, obesity, postaxial polydactyly, and a molar tooth sign on brain MRI (13).

To discuss whether these male patients with hemizygous truncating *OFD1* mutations would have different conditions (OFD1, SGBS2, or JBTS10) or belong to the same syndrome spectrum, we have created a comprehensive list of clinical manifestations in all of them (Table 2) (7, 10, 13). Macrocephaly, polydactyly (postaxial), respiratory insufficiency with recurrent respiratory tract infections in survivors, and severe mental or developmental retardation were shared by all the families (7, 10, 13). Nasal bridge features (depressed or broad) and lip abnormalities (cleft lip, pseudocleft lip, full lips, and prominent philtrum) were shared by the families with OFD1 and JBTS10 (7, 13). Brain malformations including hypoplasia or agenesis of corpus callosum, hypoplasia or agenesis cerebellar vermis as well as posterior fossa abnormalities (large, occipital encephalocele) were also shared by the families with OFD1 and JBTS10 (7, 13). III-5 in the present family was described to have Dandy-Walker malformation on brain ultrasonography. Three patients with JBTS10 were described to have a molar tooth sign on brain MRI, which is the characteristic neuroradiological hallmark of Joubert syndrome (13). Dandy-Walker malformation, typically consisting of agenesis or hypoplasia of cerebellar vermis, a cystic dilatation of the fourth ventricle, and an enlarged posterior fossa with a high position of the tentorium, is usually distinguishable from Joubert syndrome, characterized anatomically by agenesis or hypoplasia of cerebellar vermis and enlargement of the superior cerebellar peduncles and deep interpeduncular fossa resulting from a lack of normal decussation of superior cerebellar peduncular fiber tracts, leading to the characteristic 'molar tooth' appearance on transverse computed tomography and MRI of the midbrain (14); and clinically by hypotonia, developmental retardation, abnormal respiratory patterns, and oculomotor apraxia (15). However, Joubert syndrome could be present in association with Dandy-Walker malformation (15); and in such a case, Dandy-Walker malformation was reported to have initially masked the molar tooth sign because of a cystic dilatation of the fourth ventricle (16). Some authors state that the presence of the molar tooth sign does not, in itself, allow a diagnosis, Joubert syndrome, to be made; but that clinical evidence of the syndrome including hypotonia and developmental retardation accompanied by either abnormal breathing or abnormal eye movements should be present (14, 17). Typical respiratory abnormalities in Joubert syndrome, represented by short alternate episodes of apnea and hyperpnea or episodic hyperpnea alone (18), were not described in the patients with JBTS10, with only one presenting with stridor and intermittent cyanosis soon after birth (13). Abnormal eye movements including oculomotor apraxia were not mentioned in those with JBTS10 (13). In view of these evidences, it is reasonable to consider that the male patients with *OFD1* mutations, identified to date, would belong to a clinical continuum with wide intra- and inter-familial phenotypic variations of a single disorder.

A review by Macca and Franco (4) summarized all reported mutations in OFD1 patients. In total, 99 different mutations (7 genomic deletions and 92 point mutations) were identified, including 67 frameshift mutations (58%), 14 missense mutations (12%), 14 splice-site mutations (12%), 13 nonsense mutations (11%), and an in-frame deletion. Point mutations occur only in the first 17 exons (*OFD1* consists of 23 exons). A significant genotype–phenotype correlation between high-arched/cleft palate and missense and splice-site mutations has been identified (19). In addition, cystic kidney is more frequently associated with mutations in exons 9 and 12 (19). Quantitative PCR analysis of *OFD1* mRNA levels in EBV-LCLs from two families with JBTS10 showed that 30% and 58% of *OFD1* expression remained, suggesting that the mutant mRNA would be subject to nonsense-mediated decay and that the phenotypic variability observed for *OFD1* mutations would be caused by changes in activity of remaining truncated OFD1 protein (13). To date, premature stop codons at 713 in exon 16 (19), 796 in exon 17 (this report), 926 in exon 21 (13), and 956 in exon 21 (13) are associated with survival in males with hemizygous truncating *OFD1* mutations and no or subtle clinical manifestations in females with heterozygous *OFD1* mutations. Heterozygous truncating *OFD1* mutations preserving normal exons 1–16 have been reported in only two families with typical female OFD1 patients: a single-base deletion (c.2349delC in exon 17, p.Ileu784Serfs*85) (20) and a deletion of complete exon 17 (21). Mutations producing longer truncated protein (~ exon 17) might cause a milder form of the disorder that could not be detected in typical female OFD1 patients, but could be detected in male patients with multiple congenital anomalies and probable lethality in childhood.

Table 2. Clinical features of male patients with *OFD1* mutations

	Family 1 (present family)			Family 2[b]	Family 3[c]				Family 4[d] (W07-713)			Family 5[d]	Carrier
Patient	II-4	III-1	III-5	1	IV-1	IV-3	IV-11	6 Patients	III-9	IV-10	6 Patients	(UW87)	19 Females
Age	0d/D	14d/D	1d/D		11 y	18 m/D	3 y/D	D	34 y	3.5 y	D (3)		
Birth weight (g) (gestational age)	2056 (33)	3064 (39)	1704 (32)		3850 (40)	4120 (38)	1915 (35)			3050 (Te)		4090 (41)	
Macrocephaly (>1.5 SD)	+		+		+	+	+	Some				+	
Obesity					+				–	–	–	+	
Craniofacial (87.3%[a])									–	–	–		
Facial anomalies (69.1%[a])													
Prominent forehead	+		+										
Redundant neck skin	+											+	
Hypertelorism	+	+	+	+									
Epicanthus		+											
Short palpebral fissures	+	+											
Nasal bridge features	Dep		Dep						Br	Br		Dep	
Low-set ears	+	+			+				+	+			
Lip abnormalities (32.6%[a])	PCL	CL	PCL	PCL					F_L, PP	F_L, PP		PCL	PCL (1)
Oral													
Palatal abnormalities (49.6%[a])	CSP	CP	CSP	CSP	HP								
Accessory frenulae (63.7%[a])													+ (4)
Tongue abnormalities (84.1%[a])	Nar											MG	Lob (3)
Teeth abnormalities (43.3%[a])													Ir (1)
Skeletal													
Short fingers/brachydactyly					+		+			–		+	
Postaxial polydactyly (3.7%[a])	LtH	BiH		BiHRtBLT		RtH			–	BiHF	BiHF (4)	BiHLtF	
Preaxial polydactyly (19.3%[a])	BiBrHx	BiF		BiBHx	BiBrT								
Respiratory													
Laryngeal anomalies	+												
Respiratory insufficiency	+	+				+				+			
Recurrent infections					+	+	+	+	+	+	+ (6)	+	
Cardiovascular													
Congenital heart defects	ASD, PDA	AVSD	HLHS	AVSD						–			
Genitourinary													
Cystic kidney	–		–		–	–			–	–	–	–	
Urinary tract abnormalities	HU	EUO											
Genital abnormalities	MP, C												
Gastrointestinal													
Esophageal abnormalities			+										
Ophthalmological													
Microphthalmia/microcornea	+												
Persistent papillary membrane		+											

Table 2. Continued

Patient	Family 1 (present family)			Family 2[b]	Family 3[c]				Family 4[d] (W07-713)			Family 5[d]	Carrier
	II-4	III-1	III-5	1	IV-1	IV-3	IV-11	6 Patients	III-9	IV-10	6 Patients	(UW87)	19 Females
Optic disc coloboma		+											
Optic nerve atrophy												+	
Retinal detachment	+												
Retinitis pigmentosa									+	+	+ (1)	−	
Central nervous system (48.4%[a])													
Hydrocephalus		+	+	+	−	−	+						
Gyrus abnormalities	Hp			PM	−	−	−						
Corpus callosum abnormalities		Ag		Ag	−	−	−					Hp	
Cerebellar vermis abnormalities		Ag	Ag		−	−	−		Hp	Hp			
Thick superior cerebellar peduncles					−	−	−		+	+			
Molar tooth sign					−	−	−		+	+		+	
Dandy-Walker malformation			+		−	−	−						
Posterior fossa abnormalities				L	−	−	−			L		EC	
Developmental/mental retardation					S	S	+	S	S	S	+ (All)	S	

+, present; −, absent; blank, data not available; Ag, agenesis; ASD, atrial septal defect; AVSD, atrioventricular septal defect; BHx, bifid halluces; Bi, bilateral; BLT, bifid little toe; Br, broad; C, cryptorchidism; CL, cleft lip; CP, cleft palate; CSP, cleft soft palate; d, days; D, death; Dep, depressed; EC, encephalocele; EUO, ectopic urethral opening; F, foot/feet; FL, full lips; H, hand(s); HF, hands and feet; HLHS, hypoplastic left heart; Hp, hypoplasia; HP, high palate; HU, hydroureter; Hx, halluces; Ir, irregular; L, large; Lob, lobulated; Lt, left; m, months; MG, midline groove; MP, micropenis; Nar, narrowing of the tip of the tongue; PCL, pseudocleft of the upper lip; PDA, patent ductus arteriosus; PM, polymicrogyria; PP, prominent philtrum; Rt, right; S, severe; Te, term; T, thumbs; y, years.

[a]From Macca and Franco (4).

[b]From Goodship et al. (7).

[c]From Budny et al. (10).

[d]From Coene et al. (13).

High-throughput, next-generation sequencing (NGS) has had a tremendous impact on human genetic research (22). Moreover, techniques enabling enrichment of selected regions enable us to use NGS efficiently and to identify the causative genes for a reasonable number of genetic disorders as well as susceptibility genes for complex diseases and health-related traits (23). In particular, X-linked disorders are good candidates for exome sequencing. We recently identified a nonsense mutation in *MCT8* causing X-linked leukoencephalopathy in a family from only two affected male samples (24). We have also identified two possible but inconclusive missense variants (*L1CAM* and *TMEM187*) in a family with an atypical X-linked leukodystrophy from only two affected male samples (25). In this study, exome sequencing accompanied by appropriate bioinformatics techniques and a co-segregation evaluation successfully revealed a disease-causing mutation in *OFD1*, which could not have been assumed to be a candidate based on the clinical manifestations of the affected male patients. Unbiased rapid screening through these technologies is a powerful method for the detection of mutations in unexpected causative genes in undiagnosed patients with multiple congenital malformations.

In conclusion, we have identified a causative splicing mutation in *OFD1*, through exome sequencing, in a family with three males having an 'unclassified' X-linked lethal congenital malformation syndrome. The affected males manifested severe multisystem complications in addition to the cardinal features of OFD1 and the carrier female showed only subtle features of OFD1. The present patients, as well as the previously reported male patients from four families (one with clinical OFD1; one with SGBS2 and an *OFD1* mutation; two with JBTS10 and *OFD1* mutations), would belong to a single syndrome spectrum caused by truncating *OFD1* mutations, presenting with craniofacial features (macrocephaly, depressed or broad nasal bridge, and lip abnormalities), postaxial polydactyly, respiratory insufficiency with recurrent respiratory tract infections in survivors, severe mental or developmental retardation, and brain malformations (hypoplasia or agenesis of corpus callosum and/or cerebellar vermis and posterior fossa abnormalities).

Acknowledgements

The authors are grateful to the family for their participation in this study. The authors are also thankful to Prof Germana Meroni (Cluster in Biomedicine, Trieste) for mutation analysis of *MID1*, Dr Takeshi Futatani (Department of Pediatrics, Toyama Prefectural Central Hospital, Toyama, Japan), Dr Masahiko Kawabata (Department of Internal Medicine, Toyama Prefectural Central Hospital, Toyama, Japan), and Dr Akio Uchiyama (Department of Pathology, Toyama Prefectural Central Hospital, Toyama, Japan) for collecting clinical information; Dr Gen Nishimura (Department of Radiology, Tokyo Metropolitan Children's Medical Center) for helping radiological assessment; and Miss Junko Kunimi (Department of Medical Genetics, Shinshu University School of Medicine, Matsumoto, Japan) and Dr Shin-ya Nishio (Department of Otolaryngology, Shinshu University School of Medicine, Matsumoto, Japan) for their technical assistance. This work was supported by research grants from the Ministry of Health, Labour and Welfare (T. K., Y. F., H. S., N. Mi., and N. Ma.), the Japan Science and Technology Agency (N. Ma.), the Strategic Research Program for Brain Sciences (N. Ma.) and a Grant-in-Aid for Scientific Research on Innovative Areas (Foundation of Synapse and Neurocircuit Pathology) from the Ministry of Education, Culture, Sports, Science and Technology of Japan (N. Ma.), a Grant-in-Aid for Scientific Research from Japan Society for the Promotion of Science (N. Ma.), a Grant-in-Aid for Young Scientist from Japan Society for the Promotion of Science (H. S. and N. Mi.) and a grant from the Takeda Science Foundation (N. Mi. and N. Ma.). This work was performed at the Advanced Medical Research Center, Yokohama City University, Japan.

Y. T., H. D., H. S., and N. Mi. performed the genetic analysis; T. K., K. H., Y. N., K. W., and Y. F. evaluated clinical aspects of the family, recruited samples, and prepared them for the analysis. Y. T., T. K. and N. Ma. wrote the manuscript.

Ethics approval

The work was approved by the Yokohama City University (Faculty of Medicine) and the Shinshu University (School of Medicine). Patient consent was obtained.

References

1. Papillon-Leage M, Psaume J. Une malformation hereditaire de la muquese buccale: brides et freins anomaux. Rev Stomatol 1954: 55: 209–227.
2. Gorlin RJ, Psaume J. Orofaciodigital dysostosis: a new syndrome. A study of 22 cases. J Pediatr 1962: 61: 520–530.
3. Ferrante MI, Giorgio G, Feather SA et al. Identification of the gene for oral-facial-digital type I syndrome. Am J Hum Genet 2001: 68: 569–576.
4. Macca M, Franco B. The molecular basis of oral-facial-digital syndrome, type 1. Am J Med Genet C 2009: 151C: 318–325.
5. Toriello HV, Franco B. Oral-facial-digital syndrome type I. In: Pagon RA, Bind TD, Dolan CR, Stephans K, Adam MP, eds. GeneReviews at genetests: Medical Genetics Information Resource (database online). Seattle, WA: Copyright, University of Washington, 1993–2011, from http://www.genetests.org. Accessed on July 23, 2011.
6. Morleo M, Franco B. Dosage compensation of the mammalian X-chromosome influences the phenotypic variability of X-linked dominant male-lethal disorders. J Med Genet 2008: 45: 401–408.
7. Goodship J, Platt J, Smith R, Burn J. A male with type I orofaciodigital syndrome. J Med Genet 1991: 28: 691–694.
8. Fontanella B, Russolillo G, Meroni G. MID1 mutations in patients with X-linked Opitz G/BBB syndrome. Hum Mutat 2008: 29: 584–594.
9. Nishimura-Tadaki A, Wada T, Bano G et al. Breakpoint determination of X;autosome balanced translocations in four patients with premature ovarian failure. J Hum Genet 2011: 56: 156–160.
10. Budny B, Chen W, Omran H et al. A novel X-linked recessive mental retardation syndrome comprising macrocephaly and ciliary dysfunction is allelic to oral-facial-digital type I syndrome. Hum Genet 2006: 120: 171–178.
11. Terespolsky D, Farrrell SA, Siegel-Bartelt J, Weksberg R. Infantile lethal variant of Simpson-Golabi-Behmel syndrome associated with hydrops fetalis. Am J Med Genet 1995: 59: 329–333.
12. Brzustowicz LM, Farrell S, Khan MB, Weksberg R. Mapping of a new SGBS locus to chromosome Xp22 in a family with a severe form of Simpson-Golabi-Behmel syndrome. Am J Hum Genet 1999: 65: 779–783.
13. Coene KL, Roepman R, Doherty D et al. OFD1 is mutated in X-linked Joubert syndrome and interacts with LCA5-encoded lebercilin. Am J Hum Genet 2009: 85: 465–481.
14. McGraw P. The molar tooth sign. Radiology 2002: 229: 671–672.
15. Chance PF, Cavalier L, Satran D, Pellegrino JE, Koenig M, Dobyns WB. Clinical nosologic and genetic aspects of Joubert and related syndromes. J Child Neurol 1999: 14: 660–666.

16. Sartori S, Ludwig K, Fortuna M et al. Dandy-Walker malformation masking the molar tooth sign: an illustrative case with magnetic resonance imaging follow-up. J Child Neurol 2010: 25: 1419–1422.
17. Barkovich AJ. Anomalies with cerebellar dysgenesis: vermian dysgenesis. In: Barkovich AJ, ed. Pediatric neuroimaging, 4th edn. Lippincott Williams & Wilkins, Philadelphia 2005: 391–396.
18. Brancati F, Dallapiccola B, Valente EM. Joubert syndrome and related disorders. Orphanet J Rare Dis 2010: 5: 20.
19. Prattichizzo C, Macca M, Novelli V et al. Mutational spectrum of the oral-facial-digital type I syndrome: a study on a large collection of patients. Hum Mutat 2008: 29: 1237–1246.
20. Thauvin-Robinet C, Cossée M, Cormier-Daire V et al. Clinical, molecular, and genotype-penotype correlation studies from 25 cases of oral-facial-digital syndrome type 1: a French and Belgian collaborative study. J Med Genet 2006: 43: 54–61.
21. Thauvin-Robinet C, Franco B, Saugier-Veber P et al. Genomic deletions of *OFD1* account for 23% of oral-facial-digital type 1 syndrome after negative DNA sequencing. Hum Mutat 2008: 30: E320–E329.
22. Shendure J, Ji H. Next-generation DNA sequencing. Nat Biotechnol 2008: 26: 1135–1145.
23. Bamshad MJ, Ng SB, Bigham AW et al. Exome sequencing as a tool for Mendelian disease gene discovery. Nat Rev Genet 2011: 12: 745–755.
24. Tsurusaki Y, Osaka H, Hamanoue H et al. Rapid detection of a mutation causing X-linked leukodystrophy by exome sequencing. J Med Genet 2011: 48: 606–609.
25. Tsurusaki Y, Okamoto N, Suzuki Y et al. Exome sequencing of two patients in a family with atypical X-linked leukodystrophy. Clin Genet 2011: 80: 161–166.

Gain-of-Function Mutations in *RIT1* Cause Noonan Syndrome, a RAS/MAPK Pathway Syndrome

Yoko Aoki,[1,*] Tetsuya Niihori,[1] Toshihiro Banjo,[2] Nobuhiko Okamoto,[3] Seiji Mizuno,[4] Kenji Kurosawa,[5] Tsutomu Ogata,[6] Fumio Takada,[7] Michihiro Yano,[8] Toru Ando,[9] Tadataka Hoshika,[10] Christopher Barnett,[11,12] Hirofumi Ohashi,[13] Hiroshi Kawame,[14] Tomonobu Hasegawa,[15] Takahiro Okutani,[16] Tatsuo Nagashima,[17] Satoshi Hasegawa,[18] Ryo Funayama,[19] Takeshi Nagashima,[19] Keiko Nakayama,[19] Shin-ichi Inoue,[1] Yusuke Watanabe,[2] Toshihiko Ogura,[2] and Yoichi Matsubara[1,20]

RAS GTPases mediate a wide variety of cellular functions, including cell proliferation, survival, and differentiation. Recent studies have revealed that germline mutations and mosaicism for classical RAS mutations, including those in *HRAS*, *KRAS*, and *NRAS*, cause a wide spectrum of genetic disorders. These include Noonan syndrome and related disorders (RAS/mitogen-activated protein kinase [RAS/MAPK] pathway syndromes, or RASopathies), nevus sebaceous, and Schimmelpenning syndrome. In the present study, we identified a total of nine missense, nonsynonymous mutations in *RIT1*, encoding a member of the RAS subfamily, in 17 of 180 individuals (9%) with Noonan syndrome or a related condition but with no detectable mutations in known Noonan-related genes. Clinical manifestations in the *RIT1*-mutation-positive individuals are consistent with those of Noonan syndrome, which is characterized by distinctive facial features, short stature, and congenital heart defects. Seventy percent of mutation-positive individuals presented with hypertrophic cardiomyopathy; this frequency is high relative to the overall 20% incidence in individuals with Noonan syndrome. Luciferase assays in NIH 3T3 cells showed that five RIT1 alterations identified in children with Noonan syndrome enhanced ELK1 transactivation. The introduction of mRNAs of mutant *RIT1* into 1-cell-stage zebrafish embryos was found to result in a significant increase of embryos with craniofacial abnormalities, incomplete looping, a hypoplastic chamber in the heart, and an elongated yolk sac. These results demonstrate that gain-of-function mutations in *RIT1* cause Noonan syndrome and show a similar biological effect to mutations in other RASopathy-related genes.

RAS GTPases are monomeric G proteins with a molecular mass of 20–40 kDa and cycle between a GTP-bound active and a GDP-bound inactive state. The members of the RAS superfamily are structurally classified into at least five subfamilies: RAS, Rho, Rab, Sar1/Arf, and Ran families.[1,2] The Ras subfamily consists of classical RAS proteins (HRAS, KRAS, and NRAS), RRAS, RRAS2 (TC21), RRAS3 (MRAS), RAPs, RAEB, RALs, RIT1, and RIT2 (RIN). RAS proteins interact with multiple effectors, including RAF kinases, phosphatidylinositol 3-kinase (PI-3 kinase), RalGDS, p120GAP, MEKK1, RIN1, AF-6, phospholipase C epsilon, and the Nore-MST1 complex, and activate multiple downstream signaling cascades.[1,2] Of these signaling pathways, the RAS/mitogen-activated protein kinase (RAS/MAPK) signaling pathway plays a central role in cellular proliferation and differentiation.

Noonan syndrome (MIM 163950) is an autosomal-dominant disorder characterized by short stature, distinctive facial features, and congenital heart defects.[3,4] The distinctive facial features include hypertelorism, downslanting palpebral fissures, ptosis, a webbed or short neck, and low-set, posteriorly rotated ears. Congenital heart defects, including pulmonary valve stenosis and atrial septal defects, occur in 50%–80% of individuals. Hypertrophic cardiomyopathy is observed in 20% of affected individuals. Other clinical manifestations include cryptorchidism, mild intellectual disability, bleeding tendency, and hydrops fetalis. The incidence of this syndrome is estimated to be between 1 in 1,000 to 1 in 2,500 live births. Individuals with Noonan syndrome are at risk of juvenile myelomonocytic leukemia (JMML), a myeloproliferative disorder characterized by excessive production of myelomonocytic cells.[4] Noonan syndrome exhibits phenotypic overlap

[1]Department of Medical Genetics, Tohoku University School of Medicine, Sendai 980-8574, Japan; [2]Department of Developmental Neurobiology, Institute of Development, Aging, and Cancer, Tohoku University, Sendai 980-8575, Japan; [3]Department of Medical Genetics, Osaka Medical Center and Research Institute for Maternal and Child Health, Izumi 594-1101, Japan; [4]Department of Pediatrics, Central Hospital, Aichi Human Service Center, Kasugai 480-0392, Japan; [5]Division of Medical Genetics, Kanagawa Children's Medical Center, Yokohama 232-8555, Japan; [6]Department of Pediatrics, Hamamatsu University School of Medicine, Hamamatsu 431-3192, Japan; [7]Department of Medical Genetics, Kitasato University Graduate School of Medical Sciences, Sagamihara 252-0373, Japan; [8]Department of Pediatrics, Akita University School of Medicine, Akita 010-8543, Japan; [9]Department of Pediatrics, Municipal Tsuruga Hospital, Tsuruga 914-8502, Japan; [10]Department of Pediatrics, Tottori Prefectural Central Hospital, Tottori 680-0901, Japan; [11]South Australian Clinical Genetics Service, SA Pathology, Women's and Children's Hospital, North Adelaide, Adelaide, SA 5006, Australia; [12]School of Paediatrics and Reproductive Health, University of Adelaide, Adelaide, SA 5005, Australia; [13]Division of Medical Genetics, Saitama Children's Medical Center, Saitama 339-8551, Japan; [14]Department of Genetic Counseling, Ochanomizu University, Tokyo 112-8610, Japan; [15]Department of Pediatrics Keio University School of Medicine, Tokyo 160-8582, Japan; [16]Division of Neonatal Intensive Care Unit, General Perinatal Medical Center, Wakayama Medical University, Wakayama 641-8510, Japan; [17]Department of Pediatrics, Jikei University School of Medicine, Tokyo 105-8461, Japan; [18]Department of Pediatrics, Niigata Graduate School of Medical and Dental Sciences, Niigata 951-8510, Japan; [19]Division of Cell Proliferation, United Centers for Advanced Research and Translational Medicine, Tohoku University Graduate School of Medicine, Sendai 980-8575, Japan; [20]National Research Institute for Child Health and Development, Tokyo 157-8535, Japan
*Correspondence: aokiy@med.tohoku.ac.jp
http://dx.doi.org/10.1016/j.ajhg.2013.05.021.

with Costello syndrome (MIM 218040) and cardiofaciocutaneous (CFC) syndrome (MIM 115150).

In 2001, Tartaglia et al. identified missense mutations in protein-tyrosine phosphatase, nonreceptor type 11 (*PTPN11* [MIM 176876]), which encodes the tyrosine phosphatase SHP-2 in 50% of individuals with Noonan syndrome.[5] In contrast, loss-of-function or dominant-negative mutations in *PTPN11* have been reported in individuals with Noonan syndrome with multiple lentigines[6] (formerly referred to as LEOPARD [multiple lentigines, electrocardiographic conduction abnormalities, ocular hypertelorism, pulmonic stenosis, abnormal genitalia, retardation of growth, and sensorineural deafness] syndrome [MIM 151100]). To date, germline mutations in *PTPN11*, *KRAS* (MIM 190070), *SOS1* (MIM 182530), *RAF1* (MIM 164760), and *NRAS* (MIM 164790) have been identified in individuals with Noonan syndrome[7–12] (NS1 [MIM 163950], NS3 [MIM 609942], NS4 [MIM 610733], NS5 [MIM 611553], and NS6 [MIM 613224]), and mutations in *SHOC2* (MIM 602775) and *CBL* (MIM 165360) have been identified in two Noonan-syndrome-like syndromes[13–16] (NSLH [MIM 607721] and NSLL [MIM 613563], respectively) (Figure S1, available online). Moreover, we and another group have identified germline mutations in *HRAS* (MIM 190020) in individuals with Costello syndrome[17] and germline mutations in *KRAS*, *BRAF* (MIM 164757), *MAP2K1* (MIM 176872), and *MAP2K2* (MIM 601263) in individuals with CFC syndrome.[18,19] Mutations in *BRAF* have been also identified in a small percentage of individuals with Noonan syndrome (NS7 [MIM 613706]). A line of studies have shown that a group of the above genetic disorders result from dysregulation of the RAS and downstream signaling cascade (RAS/MAPK pathway syndromes, or RASopathies).[20,21] Recently, mosaicism for *KRAS* and *HRAS* mutations has been reported in nevus sebaceous and Schimmelpenning syndrome,[22] further extending a spectrum of diseases with a dysregulated RAS/MAPK pathway.

To identify genetic causes of Noonan syndrome, we recruited 180 individuals with Noonan syndrome or a related phenotype; they were negative for all coding exons in *PTPN11*, *KRAS*, *HRAS*, and *SOS1*; exons 6 and 11–16 in *BRAF*; exons 7, 14, and 17 in *RAF1*; exons 2 and 3 in *MAP2K1* and *MAP2K2*; and exon 1 in *SHOC2*. Further genetic analysis has been conducted according to their first diagnoses.[17,23–29] This study was approved by the ethics committee of Tohoku University School of Medicine. We obtained informed consent from all subjects involved in the study. We sequenced the exomes of 14 individuals whose clinical manifestations had been confirmed to be consistent with Noonan syndrome by trained dysmorphologists. Targeted enrichment was performed with the Agilent SureSelect Human All Exon v.1 Kit for four individuals and with the SureSelect Human All Exon 50Mb kit for ten individuals. Exon-enriched DNA libraries from these 14 individuals were sequenced on the Illumina Hiseq 2000 for 91 bp (v.1 kit) or 101 bp (50Mb kit). The Burrows-Wheeler Aligner (BWA) was used to align the sequence reads to the human genome (UCSC Genome Browser hg19);[30] all BWA parameters were kept at the default settings. After the removal of duplicates from the alignments, realignment around known indels, recalibration, and SNP and indel calling were performed with the Genome Analysis Toolkit (v.1.5).[31] ANNOVAR was used for annotation against the RefSeq database and dbSNP.[32] We identified approximately 10,000 nonsynonymous, nonsense, and splice-site variations and coding indels per individual (Table S1). Filtering steps using variant databases (dbSNP132 and the 1000 Genome Project database) and in-house exome data were carried out, resulting in the identification of 122–282 variants per individual. By visual inspection of the generated data, four heterozygous *RIT1* (MIM 609591; RefSeq accession number NM_006912.5) variants (c.246T>G [p.Phe82Leu], c.265T>C [p.Tyr89His], c.270G>T [p.Met90Ile], and c.284G>C [p.Gly95Ala]) were found in four individuals. Sanger sequencing validated the heterozygous state of the four variants. We did not find any other strong candidate genes in the results of exome sequencing.

RIT1 shares approximately 50% sequence identity with RAS, has an additional N-terminal extension, and does not possess a C-terminal CAAX motif, a specific motif for post-translational modification.[33,34] *RIT1* is located in chromosomal region 1q22 and consists of six exons. We analyzed an additional 166 individuals diagnosed with Noonan syndrome or a related disorder but without mutations in known genes.[17,23–29] Sanger sequencing of all coding exons in *RIT1* in the 166 individuals showed that 13 in 166 individuals had changes. Combining with the 4 in 14 individuals from exome sequencing, a total of nine missense, nonsynonymous mutations were identified in 17 of 180 (9%) individuals who were suspected to have Noonan syndrome or a related disorder (Table 1 and Figures 1A–1L). The identified germline *RIT1* mutations encode alterations located in the G1 domain (c.104G>C [p.Ser35Thr]); the switch I region, involving the G2 domain (c.170C>G [p.Ala57Gly]); and the switch II region, corresponding to RAS (c.242A>G [p.Glu81Gly], c.244T>G [p.Phe82Val], c.246T>G [p.Phe82Leu], c.247A>C [p.Thr83Pro], c.265T>C [p.Tyr89His], c.270G>T [p.Met90Ile], and c.284G>C [p.Gly95Ala]) (Figure S2). Amino acids where alterations are located are conserved among species (Figure S3). The *RIT1* mutations encode alterations clustered in the switch II region. In contrast, *HRAS* germline mutations identified in Costello syndrome are clustered at codon 12 and 13 in the region encoding the G1 domain[17] (Figure 1M). Mutations in parents were not identified in seven families. These mutations are apparently de novo, but biologic confirmation of parentage was not performed. One mutation, c.104G>C, was inherited from a mother with a Noonan syndrome phenotype (Table 1). None of these mutations were identified in 480 controls.

To assess the functional consequences of *RIT1* mutations identified in affected individuals, we introduced a

Table 1. Mutations in *RIT1*, Family Status, and Heart Defects of Mutation-Positive Individuals

Subject	Exon	Nucleotide Change[a]	Amino Acid Change[b]	Father	Mother	HCM[c]	PS[c]	Other Heart Defects[c]
NS414	2	c.104G>C	p.Ser35Thr	WT	p.Ser35Thr	+	–	MVP, MR
KCC27	2	c.104G>C	p.Ser35Thr	NA	NA	+	+	–
NS43	4	c.170C>G	p.Ala57Gly	NA	NA	+	–	MR, TR
NS185	4	c.170C>G	p.Ala57Gly	NA	NA	+	+	ASD, PDA
NS216	4	c.170C>G	p.Ala57Gly	NA	NA	+	–	–
NS402	4	c.170C>G	p.Ala57Gly	WT	WT	+	+	–
NS168	5	c.242A>G	p.Glu81Gly	NA	NA	–	+	VSD
NS410	5	c.244T>G	p.Phe82Val	WT	WT	+	–	–
NS358	5	c.246T>G	p.Phe82Leu	WT	WT	–	+	ASD
NS465	5	c.246T>G	p.Phe82Leu	NA	NA	–	+	VSD
NS276	5	c.247A>C	p.Thr83Pro	WT	WT	+	+	PVC
KCC8	5	c.265T>C	p.Tyr89His	NA	NA	+	+	–
KCC38	5	c.270G>T	p.Met90Ile	WT	WT	+	+	ASD, VSD, PDA
NS234	5	c.284G>C	p.Gly95Ala	WT	WT	–	–	ASD
NS265	5	c.284G>C	p.Gly95Ala	WT	WT	+	+	–
Og22	5	c.284G>C	p.Gly95Ala	NA	NA	–	–	–
Og45	5	c.284G>C	p.Gly95Ala	NA	NA	+	+	ASD

PCR primers used for sequencing are shown in Table S3. Nucleotide changes are not located in CpG dinucleotides, suggesting that they exhibit baseline mutation rates with a phenotypic filtering effect and that only these mutations lead to this phenotype. Abbreviations are as follows: WT, wild-type; HCM, hypertrophic cardiomyopathy; PS, pulmonic stenosis; MVP, mitral valve prolapse; MR, mitral regurgitation; TR, tricuspid regurgitation; ASD, atrial septal defect; PDA, patent ductus arteriosus; VSD, ventricular septal defect; PVC, premature ventricular contraction; and NA, not available.
[a]RefSeq NM_006912.5.
[b]RefSeq NP_008843.1.
[c]HCM and heart anomalies were diagnosed by echocardiography.

single-base substitution (p.Ser35Thr, p.Ala57Gly, p.Glu81Gly, p.Phe82Leu, or p.Gly95Ala) identified in individuals with Noonan syndrome into a pCAGGS expression vector[36] harboring *RIT1* cDNA. As an experimental control, cDNAs harboring *RIT1* c.89G>T (p.Gly30Val), c.104G>C (p.Ser35Asn), and c.236A>T (p.Gln79Leu) and *Braf* c.1910T>A (p.Val637Glu) (RefSeq NM_139294), which corresponds to oncogenic p.Val600Glu in humans, were also generated. RIT1 p.Gly30Val and p.Gln79Leu correspond to oncogenic RAS alterations p.Gly12Val and p.Gln61Leu, respectively. We introduced pFR-luc, pFA2-Elk1, phRLnull-luc, and wild-type (WT) or mutant expression constructs of *RIT1* into NIH 3T3 cells to examine the transcriptional activation by ELK1,[18,33] a transcription factor that is activated by MAPK. The results revealed that compared with the WT cDNA, all *RIT1* mutations exhibited significant activation. RIT1 p.Gln79Leu, followed by p.Gly95Ala, p.Ala57Gly, p.Phe82Leu, and p.Glu81Gly, showed the highest ELK1 transactivation, as also shown in a past study[37] (Figure 2A). The c.104G>C (p.Ser35Thr) substitution was identified in two affected individuals. RIT1 p.Ser35Asn, which corresponds to dominant-negative alteration p.Ser17Asn in RAS, has been used as a dominant-negative substitution in cell experiments.[38] To examine the functional consequence of p.Ser35Thr, identified in affected individuals, we compared the ELK1 transactivation in cells expressing p.Ser35Thr and those expressing p.Ser35Asn. Enhanced ELK1 transactivation was observed in cells expressing p.Ser35Thr, but not in cells expressing p.Ser35Asn (Figure 2B). These results suggest that *RIT1* mutations identified in affected individuals were gain-of-function mutations.

RIT1 is expressed ubiquitously in embryonic and adult tissues.[33,34] *Rit1*-null mice have been shown to grow to adulthood without any apparent abnormalities;[39] hence, physiological roles of RIT1 in development remain unknown. To examine the developmental effect of identified mutations, we introduced mRNA of the WT and three *RIT1* mutations (c.236A>T [p.Gln79Leu], c.242A>G [p.Glu81Gly], and c.284G>C [p.Gly95Ala]) into 1-cell-stage zebrafish embryos and observed the phenotype at 11 hr postfertilization (hpf). An oval-shaped egg sack, a typical manifestation of the gastrulation defect, was observed in embryos expressing RIT1 alterations (Figure 3A). This characteristic shape change was also observed in zebrafish expressing gain-of-function mutations of human *NRAS*[40]. Next, we observed the phenotype at later stages (48–52 hpf) (Figure 3B and Figure S4). The introduction of the WT mRNA did not interfere with the normal development, resulting in generally normal morphology

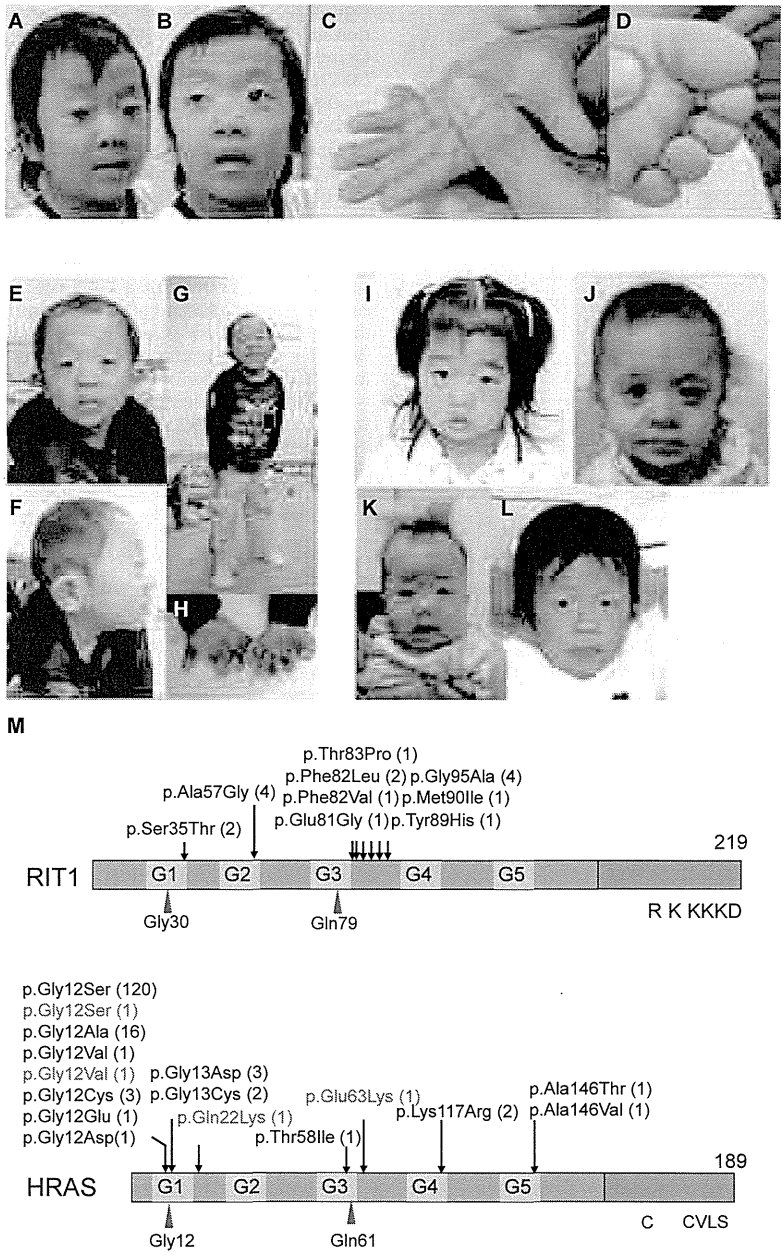

Figure 1. Photographs of Six Individuals in whom *RIT1* Mutations Were Identified
(A–D) KCC38 at 3 years of age. Broad forehead, sparse eyebrows, ptosis, hypertelorism, and hyperpigmentation were observed (A and B). Prominent finger pads were observed (C and D).
(E–H) NS358 at 4 years of age. Hypertelorism, epicanthus, sparse eyebrows, and low-set ears were observed.
(I) NS414 at 3 years of age.
(J) NS465 at 1 year of age.
(K) NS276 at 5 months.
(L) NS265 at 5 years of age.
(M) Structure and identified germline alterations in RIT1 and HRAS. HRAS alterations identified in individuals with Costello syndrome were described before[20] or shown in The RAS/MAPK Syndromes Homepage (see Web Resources). HRAS alterations identified in individuals with congenital myopathy with excess of muscle spindles[35] are indicated in purple.
We obtained specific consent for photographs from six individuals.

in 125/132 (94.7%) embryos; however, 7/132 (5.3%) embryos had limited mild craniofacial and heart abnormalities (Table 2). In contrast, a combined manifestation of craniofacial abnormalities, pericardial edema, and an elongated yolk sac was observed in 66.1%, 52.4%, and 40.5% of embryos expressing p.Gln79Leu, p.Glu81Gly, and p.Gly95Ala, respectively. Development was severely retarded in approximately 7% of embryos expressing RIT1 alterations; these embryos displayed the formation of a disorganized round body shape with a dysmorphic head and body trunk. In the head region, a hypoplastic brain, especially in the telencephalic area, was observed and resulted in misshapen morphology. In the ventral part of the head, the jaw structure was also hypoplastic, and the eyes were translocated medially. These morphological changes gave a cyclopia-like appearance. The ventral sides of the eyes were small, and coloboma along with a loss of pigment was evident (Figure 3B). These phenotypic changes are compatible with the gastrulation defect observed at 11 hpf (Figure 3A). Because the Fgf/Ras/MAPK signaling cascade plays an essential role in the convergent and extension cell movement during gastrulation,[41] perturbation by the RIT1 alterations could cause abnormal cell movement in the axial portions and thus lead to an elongated shape of the egg and the hypoplastic ventral side of the head. Detailed inspection of the morphology in mutant-injected embryos revealed abnormal cardiogenesis, namely, incomplete looping, hypoplastic chambers, and stagnation of blood flow in the yolk sac (Figure 3B). Although the atrium of these hearts beat regularly, the ventricle seemed to twitch passively by the contraction of the atrium (Movies S1, S2, S3, S4, S5, and S6). These results indicate that activating mutations in *RIT1* induce abnormal craniofacial and heart defects in zebrafish.

RIT1-mutation-positive individuals showed a distinct facial appearance, congenital heart defects, and skeletal

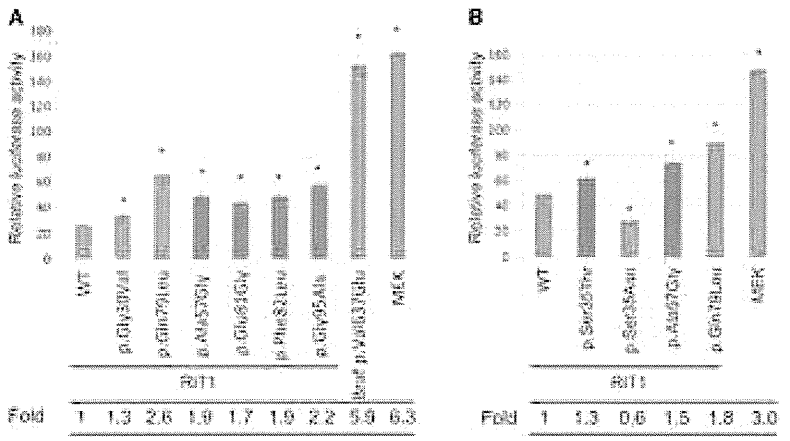

Figure 2. Stimulation of ELK Transcription in NIH 3T3 Cells Expressing *RIT1* Germline Mutations

(A) The ELK1-GAL4 vector and the GAL4 luciferase *trans*-reporter vector were transiently transfected with various *RIT1* germline mutations and activating mutations in *BRAF* and *MAP2K1* in NIH 3T3 cells. c.1910T>A (p.Val637Glu) in mouse *Braf* corresponds to oncogenic c.1799T>A (p.Val600Glu) in human *BRAF*. Relative luciferase activity was calculated by normalization to the activity of a cotransfected control vector, phRLnull-luc, containing distinguishable *R. reniformis* luciferase.

(B) ELK1 transactivation in cells expressing p.Ser35Thr, identified in individuals with Noonan syndrome, and p.Ser35Asn, were examined. p.Ser35Asn corresponds to dominant-negative alteration p.Ser17Asn in RAS.

Results are expressed as the means of quadruplicate (A) and triplicate (B) samples. Error bars represent the SDs of mean values. Red bars indicate germline *RIT1* mutations identified in Noonan syndrome. The following abbreviation is used: WT, wild-type. *$p < 0.01$ by t test.

abnormalities and were diagnosed with Noonan syndrome by diagnostic criteria developed by van der Burgt (Figures 1A–1L and Table 1).[4] Two individuals (NS358 and KCC38) were suspected to have CFC syndrome in the infantile period because of curly, sparse hair, a high cranial vault, and hypoplasia of the supraorbital ridges. Nine individuals showed perinatal abnormality, including polyhydramnios, nuchal translucency, and chylothorax (Table S2). It is of note that one individual (Og45) showing severe pleural effusion, hypertrophic cardiomyopathy, and hepatomegaly that ended in severe body edema and compromised circulation died 53 days after birth. Seven individuals showed high birth weight, probably as a result of subcutaneous edema, which is a typical manifestation observed in individuals with Noonan syndrome.[4] Out of 17 affected individuals, 16 (94%) had heart defects (Table 1): hypertrophic cardiomyopathy (HCM) in 12 (71%) individuals, pulmonary stenosis in 11 (65%) individuals, and atrial septal defects in 5 (29%) individuals. The incidence of pulmonic stenosis and mild cognitive defects is close to the overall incidence of these features in Noonan syndrome cohorts. By contrast, the incidence of HCM is far greater than in individuals with Noonan syndrome overall (25/118 in Noonan syndrome[42] versus 12/17 in individuals with *RIT1* mutations; $p < 0.0001$ by Fisher's exact test). It is of note that a high frequency of HCM (70%) was also reported in individuals with *RAF1* mutations.[10,11,24] It is possible that RIT1 interacts with RAF1 and that gain-of-function mutations in *RIT1* and *RAF1* exert similar effects in heart development.

Somatic alterations in classical RAS have been identified in approximately 30% of tumors.[43] Noonan syndrome and related disorders confer an increased risk of developing malignant tumors.[20,44] In a summary of the literature, it has been reported that 45 of 1,151 (3.9%) individuals with Noonan syndrome (but with an unknown mutation status) developed malignant tumors.[44] Since molecular analysis became available, gene-specific association with malignant tumors has been revealed. The association with JMML, a myeloproliferative disorder characterized by the excessive production of myelomonocytic cells, has been reported in individuals with *PTPN11*, *CBL*, and *KRAS* mutations. Recent reports showed that two individuals with *SOS1* mutations developed embryonal rhabdomyosarcoma.[45,46] A somatic *RIT1* variant, c.270G>A (p.Met90Ile), has been identified in lung cancer (COSMIC database). In the present cohort, 1 (NS168) of 17 individuals with *RIT1* c.242A>G (p.Glu81Gly) developed acute lymphoblastic leukemia at the age of 5 years. The child was treated by a standard protocol and has remained in complete remission. Examining whether gain-of-function mutations in *RIT1* cause tumorigenesis will require further study.

RIT1 has been isolated as a cDNA encoding highly conserved G3 and G4 domains of RAS proteins[33] or identified as a gene encoding a protein related to *Drosophila Ric*, a calmodulin-binding RAS-related GTPase.[34] RIT1 p.Gln79Leu, which corresponds to RAS p.Gln61Leu, is implicated in transforming NIH 3T3 cells, neurite outgrowth in neuronal cells, and the activation of ERK and p38 MAPK in a cell-specific manner.[37,38,47] In this study, enhanced ELK1 transactivation was observed in cells expressing mutant *RIT1* cDNAs. Previous studies showed that enhanced ELK transactivation was observed in NIH 3T3 cells expressing *HRAS*, *KRAS*, *BRAF*, and *RAF1* mutations identified in individuals with Costello, CFC, and Noonan syndromes.[17,18,24] Gastrulation defects observed in zebrafish embryos expressing RIT1 alterations (p.Glu81Gly, p.Gly95Ala, or p.Gln79Leu) were also reported in zebrafish embryos expressing an activating mutation in *NRAS*, *BRAF*, *MAP2K1*, or *MAP2K2*.[40,48] Taken together, these

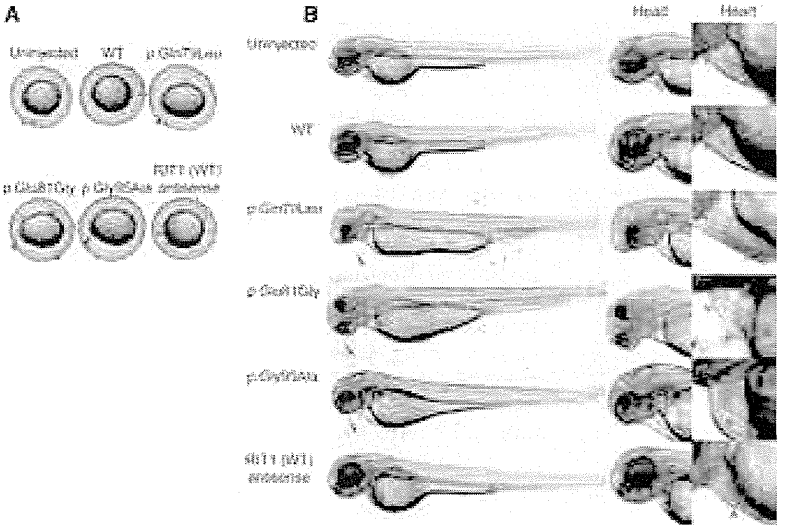

Figure 3. Morphology of Embryos Injected with the WT or Mutant *RIT1* mRNA
In vitro transcription of each mRNA was performed with the mMESSAGE mMACHINE kit (Applied Biosystems) according to the manufacturer's instructions. Synthesized mRNAs were purified with G-50 Micro Columns (GE Healthcare) and subsequently adjusted to a 300 ng/μl concentration for microinjection. Approximately 1 nl (300 pg) of RNA in water with 0.2% phenol red was injected into the cytoplasm of 1-cell-stage zebrafish embryos. Injected embryos were incubated at 28°C until observation.
(A) At 11 hpf, the shapes of the embryos injected with the WT sense or antisense mRNA were round, a normal morphology as observed in the uninjected embryos. In contrast, embryos expressing mutations (c.236A>T [p.Gln79Leu], c.242A>G [p.Glu81Gly], and c.284G>C [p.Gly95Ala]) are oval and compressed along the dorsal-ventral axis, indicative of a gastrulation defect. Note that cells have a hump in the head region at the anterior end of the body axis, the earliest manifestation of a craniofacial defect.
(B) Lateral views at 48 hpf are shown. Embryos expressing mutations (c.236A>T [p.Gln79Leu], c.242A>G [p.Glu81Gly], and c.284G>C [p.Gly95Ala]) formed swollen yolk sacs equally along the anterior posterior axis but did not show narrowing in the caudal half, which was clearly visible in the uninjected embryos and in those injected with the WT sense or antisense mRNA. In the craniofacial area, misshapen head and jaw structures and small eyes with hypoplasia on the ventral side were observed (middle panel); these phenotypes are consistent with the gastrulation defect. Shapes of the hearts (highlighted by red dotted lines) are shown in the right panel at a higher magnification. Normal looping of the heart tube and correct formation of two distinct chambers are observed in embryos injected with the WT sense or antisense mRNA. When mutations (c.236A>T [p.Gln79Leu], c.242A>G [p.Glu81Gly], and c.284G>C [p.Gly95Ala]) were expressed, looping was incomplete, resulting in stretched straight heart tubes. Constrictions at the atrial-ventricular canal are obscure, and the heart chambers are hypoplastic. Abbreviations are as follows: A, atrium; and V, ventricle.

results indicate that gain-of-function mutations in *RIT1* cause Noonan syndrome and show a similar effect to mutations in other RASopathy-related genes in human development.

Herein, we used whole-exome sequencing to identify germline *RIT1* mutations in individuals with Noonan syndrome, a disorder of the RASopathies. Mutations in *PTPN11*, *SOS1*, *RAF1*, *KRAS*, *BRAF*, and *NRAS* have been identified in 41%, 11%, 5%, 1%, 0.8%, and 0.2% of all cases, respectively,[3] and thus the frequency of *RIT1* mutations in Noonan syndrome might be similar to that of *RAF1* mutations. Our findings will improve diagnostic accuracy of Noonan syndrome and provide a clue to understanding the disorder's pathogenesis, including therapeutic approaches.

Supplemental Data

Supplemental Data include four figures, three tables, and six movies and can be found with this article online at http://www.cell.com/AJHG/.

Acknowledgments

The authors thank the families and the doctors who participated in this study. We are grateful to Jun-ichi Miyazaki at Osaka University for supplying the pCAGGS expression vector. We thank Yoko Narumi, Tomoko Kobayashi, Shoko Komatsuzaki, Yu Abe, Yuka Saito, Rumiko Izumi, Mitsuji Moriya, and Masako Yaoita for contributing to routine diagnostic work and Yoko Tateda, Kumi Kato, and Riyo Takahashi for their technical assistance. We are grateful to Eric Haan for sending samples of Noonan syndrome

Table 2. Morphologic Abnormality at 48–52 hpf of Zebrafish Embryos Injected with WT or Mutant RNA at the 1-Cell Stage

	No Abnormalities	Heart and Facial Abnormalities[a]	Severely Disorganized[b]	Total Number of Embryos
WT	125	7 (5.3%)	0 (0%)	132
p.Gln79Leu	31	78 (66.1%)	9 (7.6%)	118
p.Glu81Gly	42	55 (52.4%)	8 (7.6%)	105
p.Gly95Ala	44	34 (40.5%)	6 (7.1%)	84

[a]Craniofacial abnormalities, pericardial heart edema, and an elongated yolk sac were observed.
[b]Disorganized round body shape with a dysmorphic head and body trunk as shown in Figure S4.